International Conference on Space Optics—ICSO 2018

Chania, Greece

9–12 October 2018

Metis/Solar Orbiter polarimetric visible light channel calibration

M. Casti

S. Fineschi

G. Capobianco

M. Romoli

et al.

Metis/Solar Orbiter Polarimetric Visible Light Channel Calibration

M.Casti*[a], S. Fineschi [a], G. Capobianco [a], M. Romoli[b], E. Antonucci [a], G. Nicolini [a], G. Naletto[c], P. Nicolosi[d], D. Spadaro[e], V. Andretta[f], M. Castronuovo[g], G. Massone [a], R. Susino [a], V. Da Deppo[h], F. Frassetto[h], F. Landini[i], M. Pancrazzi[j], L. Teriaca[k], M. Uslenghi[l]

[a] INAF – Osservatorio Astrofisico di Torino, Strada Osservatorio 20, 10025 Pino Torinese, Italy;
[b] Dipartimento di Fisica e Astronomia – Università degli Studi di Firenze, Via Sansone 1, Sesto Fiorentino, Italy; [c] Departmento di Fisica e Astronomia "Galileo Galilei" - Università di Padova,Via Marzolo, 8 I-35131 Padova, Italy; [d] Dipartimento di Ingegneria dell'Informazione, Università di Padova, Via Gradenigo, 6/B, 35131 Padova, Italy; [e] INAF - Osservatorio Astrofisico di Catania, Via S.Sofia 78, 95123 Catania, Italy; [f] INAF - Osservatorio Astronomico di Capodimonte, Salita Moiariello, 16, 80131, Napoli, Italy; [g] ASI, Via del Politecnico 00133 Roma, Italy; [h] CNR - IFN, via Trasea 7, 35131 Padova, Italy, [i] INAF – Osservatorio Astrofisico di Arcetri, Largo E. Fermi 5, 50125 Firenze, Italy; [j] Dipartimento di Fisica e Astronomia – Università degli Studi di Firenze, Via Sansone 1, Sesto Fiorentino, Italy; [k] Max Planck Institute for Solar System Research, Justus-von-Liebig-Weg 3, 37077 Göttingen, Germany; [l] INAF - IASF, Via E. Bassini 15, 20133, Milano, Italy

ABSTRACT

Metis is the solar coronagraph of the ESA mission Solar Orbiter. For the first time, Metis will acquire simultaneous images of the solar corona in linearly polarized, broadband visible light (580-640 nm) and in the narrow-band HI Ly-α line (121.6 nm). The visible light path includes a polarimeter, designed to observe and analyse the K-corona linearly polarized by Thomson scattering. The polarimeter comprises a liquid crystal Polarization Modulation Package (PMP) together with a quarter-wave retarder and a linear polarizer. The Metis PMP consists of two Anti-Parallel Nematic Liquid Crystal Variable Retarders (LCVRs) with their fast axis parallel with respect to each other and a pre-tilted angle of the molecules in opposite direction. This configuration results in an instrumental wide field of view (±7°). The LCVRs provide an electro-optical modulation of the input polarized light by applying an electric field to the liquid crystal molecules inside the cells. A given optical retardance can be induced in the LCVRs by selecting a suitable voltage value. This paper reports the polarimetric characterization of the Visible-light channel for the Metis/Solar Orbiter coronagraph. The retardance-to-voltage calibration of the electro-optical polarimeter was characterized over the entire field of view of the coronagraph yielding a complete "polarimetric flat-field" of the Metis Visible-light channel.

Keywords: Solar Corona, Coronagraph, Polarization

1. INTRODUCTION

During the space era, numerous space missions have been developed aiming at better understanding solar and heliospheric physics. The upcoming mission Solar Orbiter represents the next scientific step for answering top-level science questions concerning the effects of the solar activity on the heliosphere. Despite the results obtained from the analysis of data collected by several previous missions, such as Helios, Ulysses, Yohkoh, SOHO [1], TRACE and RHESSI, there are still open questions related to the link between the Sun and the interplanetary medium. Solar Orbiter [2] [3], an European Space Agency (ESA) mission with a relevant participation from NASA, with its unique highly elliptic orbit– between 0.9 AU at aphelion and 0.28 AU at perihelion – that will be progressively more inclined to the ecliptic plane, will provide new close-up and high latitude observations of the Sun. The scientific goal of this mission is to collect data useful to understand the origin and acceleration of the solar wind, the heliospheric variability, and the role of the solar dynamo in the physics of the heliosphere. In order to achieve this result, Solar Orbiter will carry a set of ten carefully selected instruments, both remote sensing and in situ, which will provide a unique combination of measurements. Among the remote sensing instruments, Metis is the solar coronagraph.

Metis main objective is to investigate the global corona by acquiring simultaneous images in linear polarized broadband visible light (580-640 nm) and in the narrow-band (about 10 nm) around the HI Ly-α line (121.6 nm) [4] [5]. In particular, the objective of the observations obtained with the visible light channel is to characterize the hot coronal plasma by deriving the K-corona electron density from the polarized brightness with an accuracy better than 1% in the linear polarization measurements. Aiming at fully characterizing the incoming linearly polarized coronal light, a linear polarimeter composed of a quarter-wave plate, a Polarization Modulation Package (PMP) and a linear polarizer is installed in the visible path. Light modulation is performed by two Liquid Crystal Variable Retarder (LCVRs) cells [6] that constitute the Metis PMP. The LCVRs consist of optically anisotropic liquid crystal molecules embedded between two glasses of 5mm coated for one side with a transparent conductive material (indium tin oxide, ITO) and an alignment layer (rubbed polyimide) and the other side with an antireflective coating. An optical retardance in the orthogonal polarization components of the incoming light is introduced by applying an electric field that rotates the molecules, changing the cell effective birefringence. Consequently, for each voltage applied to the LCVR cells a different optical retardance angle is applied to the incoming light. One of the goals of the polarimeter calibration was to find different sets of four voltages that correspond to 90-degrees separated retardance angles. Moreover, the retardance is not homogeneous across the clear aperture and, for this reason, it was necessary to retrieve the polarimetric flat field.

This paper reports and discusses the tests performed during the calibration campaign on the proto-flight model (PFM) of the Metis polarimeter after integration into the instrument.

2. METIS CORONAGRAPH

The Metis coronagraph has been conceived to perform imaging of the solar corona (1.5 – 3 solar radii at minimum perihelion) in the visible broad band and in a narrow-band centered on the HI Ly-α line simultaneously.

Metis optical design [7] is based on an inverted external occulter (IEO) [8], which replaces the classical annular aperture of the standard solar coronagraphs. The IEO consists of a circular aperture kept by a boom at 800 mm in front of the telescope. While a spherical mirror (M0) rejects the sun disk light entering from IEO, the coronal light is collected by the imaging system, an on-axis Gregorian telescope consisting of the primary (M1) and the secondary (M2) mirror. In order to achieve the instruments goal, the M1 and M2 coating (i.e., MgF_2+Al) has been selected aiming at optimizing the reflectivity at 121.6 nm and in the visible light (VL) broad band. An internal occulter (IO) and a Lyot stop (LS) suppress the diffracted light of the edges of the IEO and M0, respectively. After the secondary mirror, an UV interference filter (IF) splits the VL and UV optical paths: the visible light is reflected back towards the polarimeter and the UV narrow band (about 10 nm) around the HI Ly 121.6 nm line is transmitted towards the UV detector.
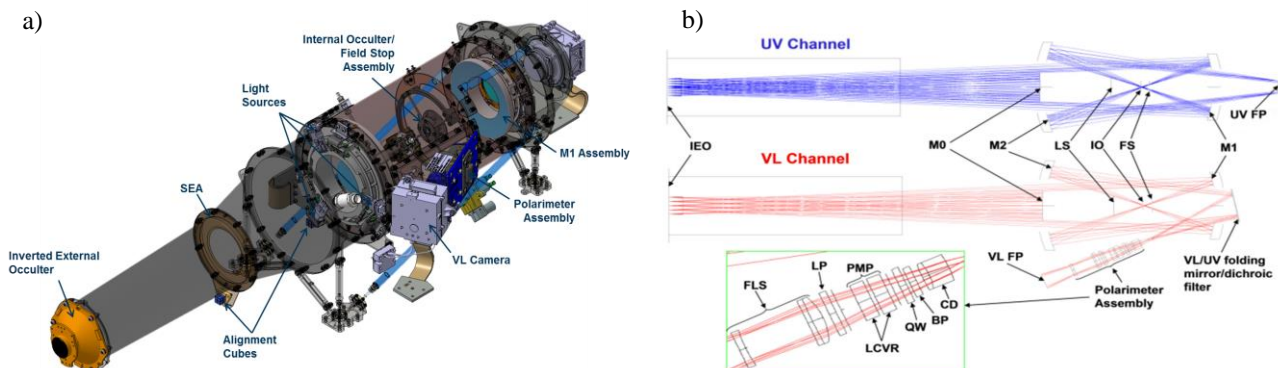
Figure 1 : Metis coronagraph: a) 3D CAD, b) Optical ray trace

The polarimetric group [9] is composed of a bandpass filter (580 – 640 nm, BP in Figure 1), a fixed achromatic quarter-wave retarder (QW), the Polarimetric Modulation Package (PMP) with the Liquid Crystal Variable Retarders (LCVRs) double-cell, and a linear polarizer (LP). These polarizing optical components are mounted in "de Senarmont configuration". If we consider a reference frame having the Z-axis in the light propagation direction, the X-axis parallel to the linear polarizer acceptance axis and the Y-axis that completes the right-handed set, the fast axis of the liquid crystal variable retarders results placed at -45° from the linear polarizer acceptance axis and the quarter-wave retarder has its fast axis at 90°. Consequently, the Mueller matrix associated with the Metis polarimeter is the product of the Mueller matrices associated with the polarizing elements inside the polarimeter.

$$M_{POL} = M_{LP} \cdot M_{PMP} \cdot M_{QW} \tag{1}$$

Where:

$$M_{LP}(\theta = 0) = \frac{1}{2} \cdot \begin{bmatrix} 1 & 1 & 0 & 0 \\ 1 & 1 & 0 & 0 \\ 0 & 0 & 0 & 0 \\ 0 & 0 & 0 & 0 \end{bmatrix} \tag{2}$$

$$M_{PMP}\left(\theta = -\frac{\pi}{4}, \delta\right) = \begin{bmatrix} 1 & 0 & 0 & 0 \\ 0 & \cos\delta & 0 & -\sin\delta \\ 0 & 0 & 1 & 0 \\ 0 & \sin\delta & 0 & \cos\delta \end{bmatrix} \tag{3}$$

$$M_{QW}\left(\theta = \frac{\pi}{2}\right) = \begin{bmatrix} 1 & 0 & 0 & 0 \\ 0 & 1 & 0 & 0 \\ 0 & 0 & 0 & 1 \\ 0 & 0 & -1 & 0 \end{bmatrix} \tag{4}$$

Consequently, the Mueller matrix associated with the Metis polarimeter is:

$$M_{POL} = \begin{bmatrix} 1 & \cos\delta & \sin\delta & 0 \\ 0 & \cos\delta & \sin\delta & 0 \\ 0 & 0 & 0 & 0 \\ 0 & 0 & 0 & 0 \end{bmatrix} \tag{5}$$

As it is possible to observe from equation (5), the last column of the retrieved Mueller matrix is composed of elements equal to zero; this proves that this configuration does not suffer from the possible presence of circularly polarized radiation. Therefore, the Stokes' vector related to the light reaching the detector is composed of three of four elements. Moreover, detectors are only sensitive to the light intensity (I), but insensitive to the values of the others Stokes parameters (Q and U). In order to retrieve the values of Q and U it is necessary to transform these parameters as a function of the light intensity. For this purpose, the incoming light is modulated by varying the voltage applied to the LCVRs and tacking exposures at four different retardance values.

3. CALIBRATION SET UP

The Metis calibration campaign took place at the National Institute for Astrophysics (INAF) Optical Payload System (OPSys) facility, hosted at the Aerospace Logistic Engineering Company (ALTEC S.p.A.), in Turin, Italy. Due to the presence of the SPace Optics Calibration Chamber (SPOCC), the OPSys laboratory is specially tailored for characterizing the optical performance of solar instruments, like coronagraphs. In fact, SPOCC is an optical test and calibration vacuum chamber provided with a Sun-simulator, a light trap and a set of baffles for stray light minimization [10].

The polarimetric calibration of the Metis visible light path was aimed at retrieving the retardance-voltage relationship for the liquid crystal cells embedded in the Metis polatimeter and the polarimetric flat fielding. In order to achieve these goals, we use two different set-ups.

The first test consisted of the VL imaging of the "Sun-disk" (extended source) at view angle of +2.2°, with the Metis polarimeter operating in vacuum conditions at 30°C. A view angle different than zero was necessary in order to avoid the stray light on the focal plan. The telescope was positioned on the SPOCC optical bench and a well-known polarized light was injected within the calibration chamber through its optical window. To perform this test, we used a VL LED source and a linear polarizer. As a result, we measured the VL polarization response for different orientations of the pre-polarizer by modulating the light using the PMP.

The goal of the second test was to characterize the polarimetric response in visible light on the overall instrument field of view. We followed the test approach described before, by selecting the incoming light polarization with a linear polarizer positioned between the light source, i.e. a flat field panel, and the telescope; the incoming radiation was then modulated by applying a suitable voltage value to the LCVR cells.

a)   b)
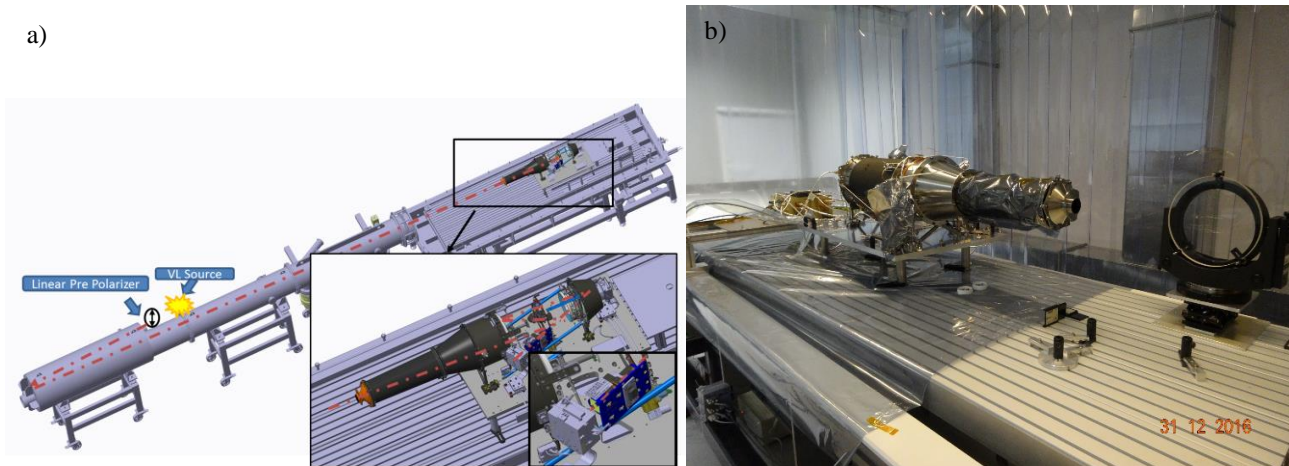
Figure 2 : Set-ups for the Metis visible light path polarimetric calibration: a) VL imaging of the "Sun-disk, b) polarimetric flat-fielding test

4. VISIBLE LIGHT CHANNEL CALIBRATION

As reported in section 3, in order to acquire data for fully characterizing the polarimetric response of the Metis VL channel, we used two different test set-ups. Consequently, the acquired images have different features, related to the performed test main goal.

The main goal of the VL imaging of the "Sun-disk" test was to characterize the VL polarimetric response of the instrument and evaluate the instrumental polarization with 1% accuracy. In order to reach this goal, we acquired data related to different polarization states of the incoming light. In particular, we used the set-up illustrated in Figure 2 (a), rotating the linear pre-polarizer in order to change the light polarization.

Figure 3 reports four images acquired during this test and related to four different voltages applied to the Metis PMP that correspond to four optical retardance angles separated by 90 degrees.
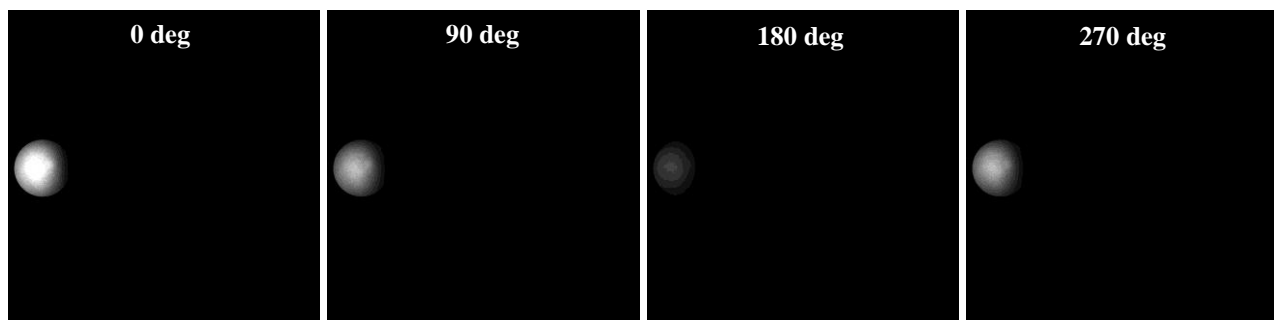
Figure 3 : Polarimetric VL imaging of the "Sun-disk" at four different optical retardance angles

In order to retrieve the intensity value associated with the acquired images, we selected an area within the Sun disk and computed the DN average. As a result, for each position of the linear pre-polarizer, we obtained the intensity vs voltage plot shows in Figure 4.
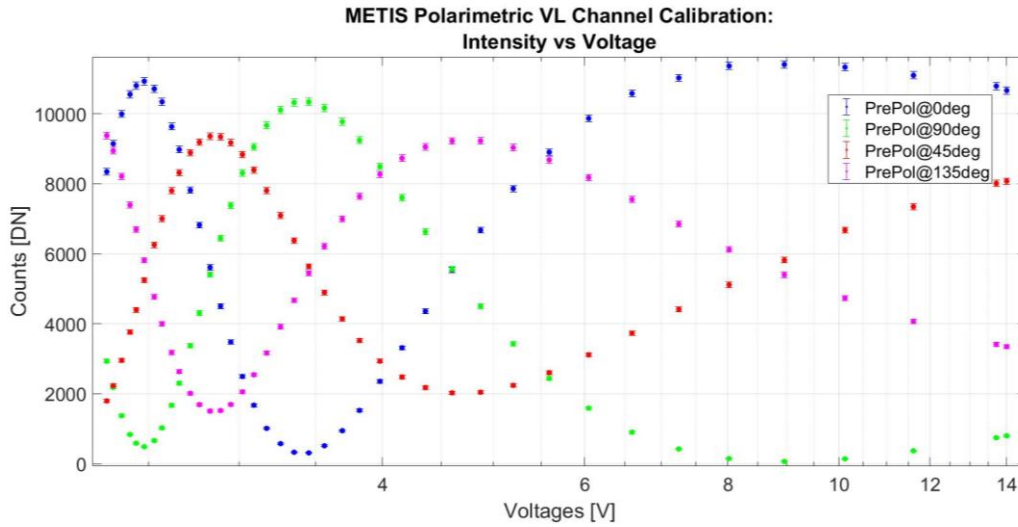
Figure 4 : Data acquired during the polarimetric VL channel calibration in vacuum

The second test was related to the instrument polarimetric flat fielding: the final goal was to characterize the polarimetric response for each detector pixel. Figure 5 reports four images acquired during this test and related to four different voltages applied to the Metis PMP that correspond to four optical retardance angles separated by 90 degrees.
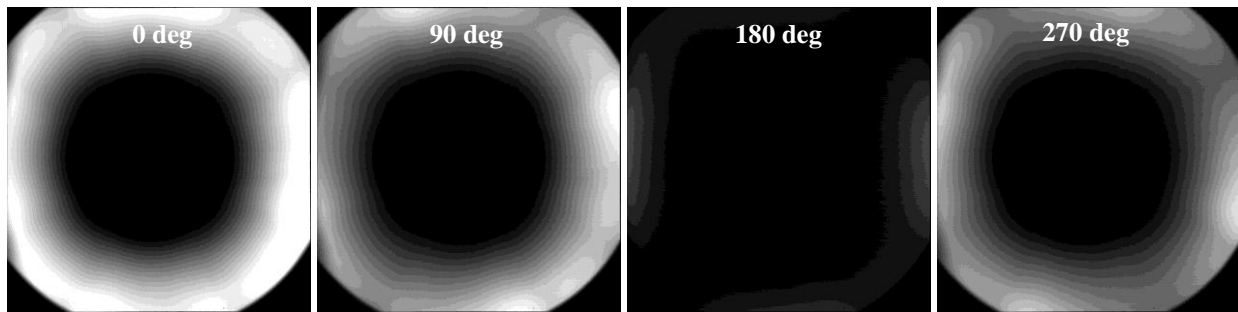
Figure 5 : Polarimetric flat fielding at four different optical retardance angles

In order to avoid spikes due to the mathematical computation, we performed the data analysis on binned flat field images (512 x 512 pixels). Moreover, for performing the analysis we considered only the area within the two circumferences shown in Figure 6. As a matter of the fact, the first circumference delimits the occulter image while the second one excludes the vignetting effects.
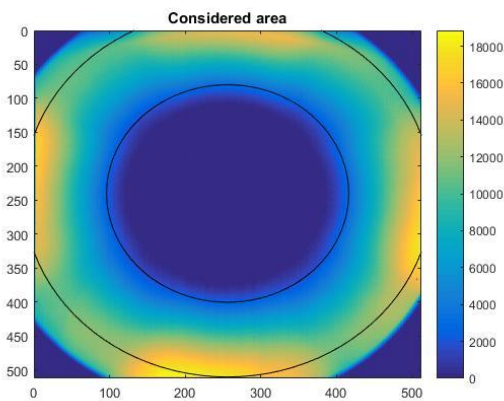
Figure 6 : Area considered for performing data analysis

5. VL SUN DISK IMAGING DATA MODELING

During a previous Metis PMP and stand-alone polarimeter calibration campaign [11], we found that double-term exponential fits well the dependence of the retardance on the voltage applied to the liquid crystal cells. As a consequence, the resulting empirical model used to describe the retardance introduced by the PMP is (6).

$$\delta(V) = a \cdot e^{b \cdot V} + c \cdot e^{d \cdot V} \tag{6}$$

If we consider the optics involved within the set-up and the PMP mathematical model, we obtain the expression of the modulation curve reported in equation (7).

$$I(V) = \frac{I_0}{2}\left\{1 + p \cdot \cos\left[\left(a \cdot e^{bV} + c \cdot e^{dV}\right) + 2\theta_{LP}\right]\right\} + k \tag{7}$$

Where I_0 represents the amplitude of the Malus curve, p is the degree of polarization of the incoming light and k is a parameter relative to the background noise.

We solved equation (7) for each position of the linear pre-polarizer, i.e. ϑ_{LP}. Figure 7 reports the obtained fitting curve related to each data set acquired at the same pre-polarizer position.
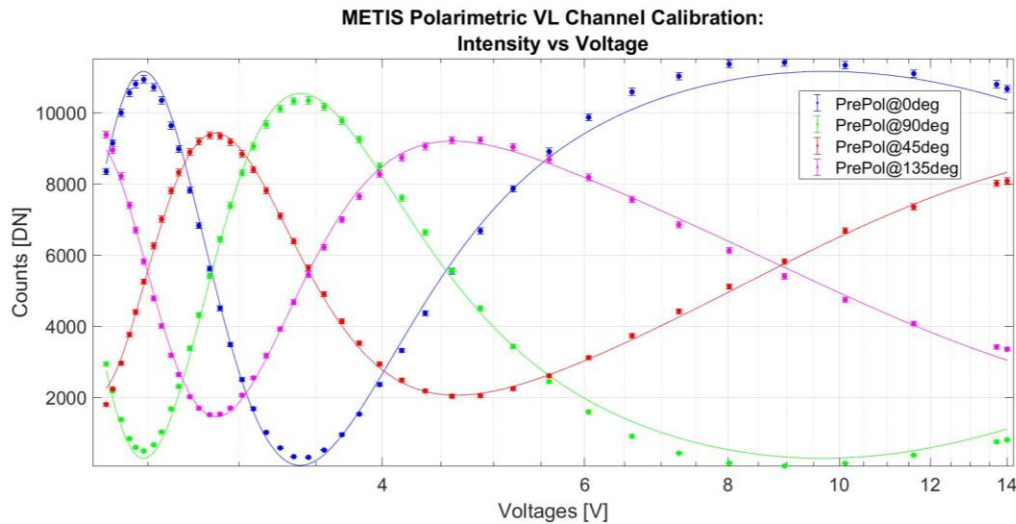
Figure 7 : Fitting curves obtained for data acquired at 30°C and related to different incoming polarized light beams

Table 1 reports the coefficient values obtained by fitting the acquired data for differently polarized incoming beams. As it is possible to see, we obtained different coefficient values of the double-exponential fitting curve – i.e., a, b, c, and d -, however they result consistent within the uncertainty.

Table 1 : Coefficients of the fitting curves obtained for data acquired at 30°C for different incoming polarized light beams

LP angle	a	b [V^{-1}]	c	d [V^{-1}]	I$_0$ [DN]	k [DN]	r-squared
45 deg	3599±604	-1.05±0.09	236±34	-0.10±0.02	22590±510	-28±195	0.996
0 deg	4417±720	-1.17±0.08	299±25	-0.13±0.01	15020±300	1983±115	0.997
-45 deg	3745±609	-1.08±0.09	247±32	-0.10±0.02	20920±440	181±149	0.996
90 deg	3879±603	-1.08±0.08	257±23	-0.11±0.01	15790±350	1375±124	0.996

The retrieved fitting curve coefficients can be used to retrieve the Malus curve associated with the analyzed dataset (Figure 8).
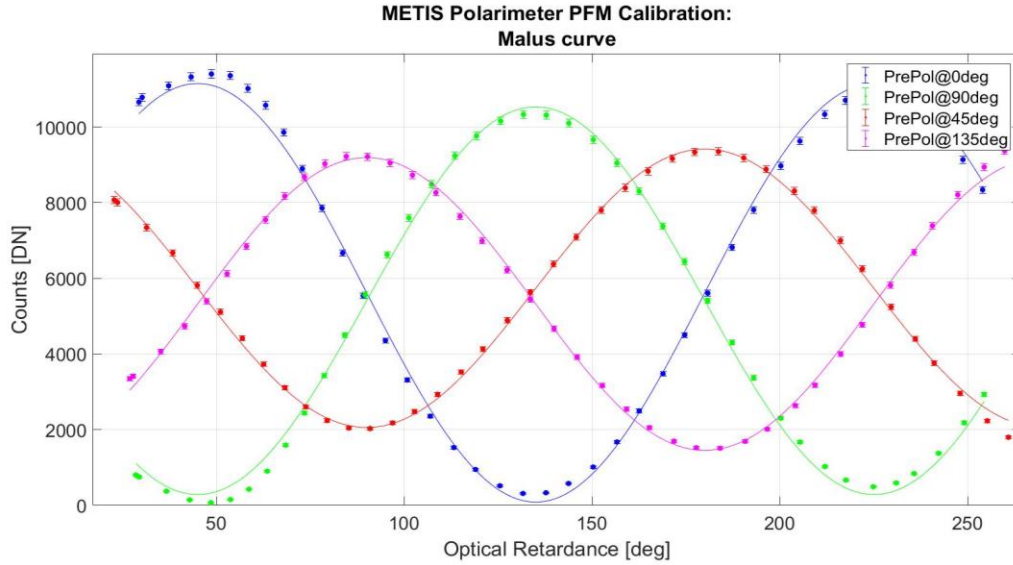
Figure 8 : Malus curves associated with data acquired with the Metis polarimeter at 30°C

As a last step, we retrieved the retardance-voltage curve, which has been modeled as per (6).
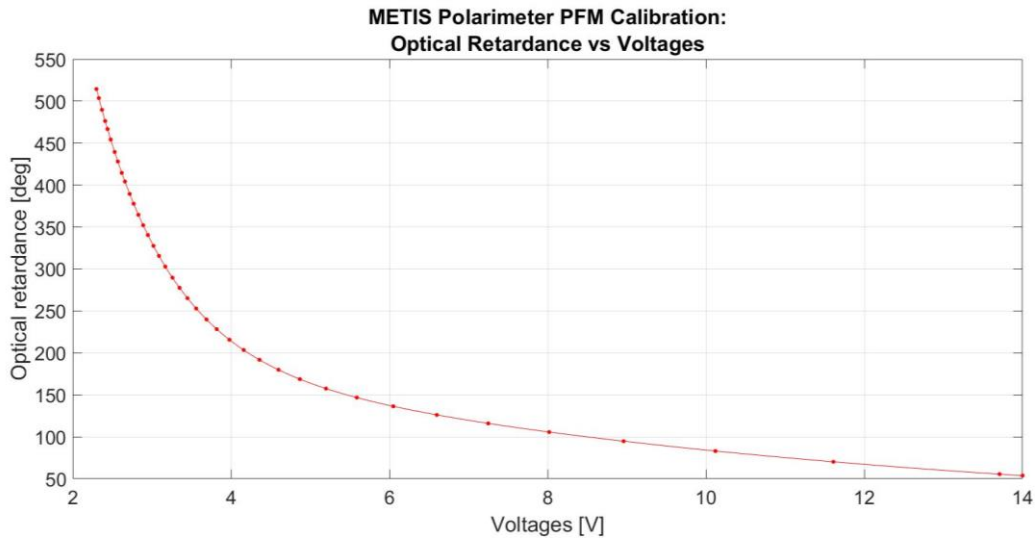
Figure 9 : Retrieved retardance vs voltage curve

6. POLARIMETRIC FLAT FIELDING DATA ANALYSIS METHOD

The analysis of data acquired during the Metis calibration campaign aims at characterizing the polarimetric response in visible light on the overall instrument field of view. This goal is achieved by retrieving the demodulation tensor associated with the Metis polarimeter. This is reached computing the modulation matrix associated with each pixel of the acquired polarimetric images and then inverting it in order to obtain the demodulation matrix [12].

The modulation matrix (X) links the Stokes vector (S) associated with the incoming light to the measured intensity values (m) as per (8).

$$m = X \cdot S$$ (8)

During the calibration activities, we acquired data related to different well-known polarized incoming light states and modulated it by applying different voltages to the LCVR cells. Therefore, for each pre-polarizer position equation (8) assumes the expression reported in equation (9), where m_i, $i=1,2,3,4$, are four different measured values of intensity.

$$\begin{bmatrix} m_1^{xdeg} \\ m_2^{xdeg} \\ m_3^{xdeg} \\ m_4^{xdeg} \end{bmatrix} = \begin{bmatrix} x_{11} & x_{12} & x_{13} \\ x_{21} & x_{22} & x_{23} \\ x_{31} & x_{32} & x_{33} \\ x_{41} & x_{42} & x_{43} \end{bmatrix} \begin{bmatrix} I^{xdeg} \\ Q^{xdeg} \\ U^{xdeg} \end{bmatrix} \tag{9}$$

Consequently, to compute the modulation matrix elements, it is possible to solve a unique linear system obtained collecting four different pre-polarizer positions and, for each of them, four measurements (10) and considering the theoretical Stokes' vector associated with the chosen pre-polarizer position. For the sake of simplicity, we consider the following angular positions: -45, 0, 45, and 90deg, with respect to the acceptance axis of the polarimeter linear polarizer.

$$\begin{bmatrix} m_1^{45} \\ m_2^{45} \\ m_3^{45} \\ m_4^{45} \\ m_1^{0} \\ m_2^{0} \\ m_3^{0} \\ m_4^{0} \\ m_1^{-45} \\ m_2^{-45} \\ m_3^{-45} \\ m_4^{-45} \\ m_1^{90} \\ m_2^{90} \\ m_3^{90} \\ m_4^{90} \end{bmatrix} = \begin{bmatrix} I^{45} & Q^{45} & U^{45} & 0 & 0 & 0 & 0 & 0 & 0 & 0 & 0 & 0 \\ 0 & 0 & 0 & I^{45} & Q^{45} & U^{45} & 0 & 0 & 0 & 0 & 0 & 0 \\ 0 & 0 & 0 & 0 & 0 & 0 & I^{45} & Q^{45} & U^{45} & 0 & 0 & 0 \\ 0 & 0 & 0 & 0 & 0 & 0 & 0 & 0 & 0 & I^{45} & Q^{45} & U^{45} \\ I^{0} & Q^{0} & U^{0} & 0 & 0 & 0 & 0 & 0 & 0 & 0 & 0 & 0 \\ 0 & 0 & 0 & I^{0} & Q^{0} & U^{0} & 0 & 0 & 0 & 0 & 0 & 0 \\ 0 & 0 & 0 & 0 & 0 & 0 & I^{0} & Q^{0} & U^{0} & 0 & 0 & 0 \\ 0 & 0 & 0 & 0 & 0 & 0 & 0 & 0 & 0 & I^{0} & Q^{0} & U^{0} \\ I^{-45} & Q^{-45} & U^{-45} & 0 & 0 & 0 & 0 & 0 & 0 & 0 & 0 & 0 \\ 0 & 0 & 0 & I^{-45} & Q^{-45} & U^{-45} & 0 & 0 & 0 & 0 & 0 & 0 \\ 0 & 0 & 0 & 0 & 0 & 0 & I^{-45} & Q^{-45} & U^{-45} & 0 & 0 & 0 \\ 0 & 0 & 0 & 0 & 0 & 0 & 0 & 0 & 0 & I^{-45} & Q^{-45} & U^{-45} \\ I^{90} & Q^{90} & U^{90} & 0 & 0 & 0 & 0 & 0 & 0 & 0 & 0 & 0 \\ 0 & 0 & 0 & I^{90} & Q^{90} & U^{90} & 0 & 0 & 0 & 0 & 0 & 0 \\ 0 & 0 & 0 & 0 & 0 & 0 & I^{90} & Q^{90} & U^{90} & 0 & 0 & 0 \\ 0 & 0 & 0 & 0 & 0 & 0 & 0 & 0 & 0 & I^{90} & Q^{90} & U^{90} \end{bmatrix} \begin{bmatrix} x_{11} \\ x_{12} \\ x_{13} \\ x_{21} \\ x_{22} \\ x_{23} \\ x_{31} \\ x_{32} \\ x_{33} \\ x_{41} \\ x_{42} \\ x_{43} \end{bmatrix} \tag{10}$$

Moreover, the modulation matrix is related to the polarizing elements Mueller matrix by equation (11).

$$\begin{pmatrix} m_1 \\ m_2 \\ m_3 \\ m_4 \end{pmatrix} = \begin{bmatrix} M_{11}^1 & M_{12}^1 & M_{13}^1 & M_{14}^1 \\ M_{11}^2 & M_{12}^2 & M_{13}^2 & M_{14}^2 \\ M_{11}^3 & M_{12}^3 & M_{13}^3 & M_{14}^3 \\ M_{11}^4 & M_{12}^4 & M_{13}^4 & M_{14}^4 \end{bmatrix} \begin{pmatrix} I \\ Q \\ U \\ V \end{pmatrix} = X \cdot S \tag{11}$$

Consequently, in our case study, the modulation matrix will be composed of the elements reported in equation (12), where δ is the optical retardance angle applied by the polarimeter to the input light.

$$X = \frac{1}{2} \begin{bmatrix} 1 & \cos\delta_1 & \sin\delta_1 & 0 \\ 1 & \cos\delta_2 & \sin\delta_2 & 0 \\ 1 & \cos\delta_3 & \sin\delta_3 & 0 \\ 1 & \cos\delta_4 & \sin\delta_4 & 0 \end{bmatrix} \tag{12}$$

As it is possible to observe from equation (12), the polarimeter modulation matrix shows that the Metis polarimeter does not detect the possible presence of circularly polarized radiation; we cannot retrieve information related to the V element of the incoming light Stokes vector.

By inverting equation (11), we retrieve the mathematical expression of the Stokes parameters.

$$\begin{pmatrix} I \\ Q \\ U \\ V \end{pmatrix} = X^{+} \begin{pmatrix} m_1 \\ m_2 \\ m_3 \\ m_4 \end{pmatrix}$$

(13)

7. RESULTS

The final goal of our study is the polarimetric characterization of the VL channel. This means to retrieve the demodulation tensor associated with the Metis polarimeter as the composition of the demodulation matrix elements related to each pixel. This will allow us to characterize the incoming light, under a polarimetric point of view, from the light intensity. The first step is to retrieve the modulation tensor. The elements of the theoretical modulation matrix are reported in (12). If we considered the optical retardance angles δ = 0, 90, 180, and 270deg, the modulation matrix assumes the values reported in (14). We retrieve the voltages associated with the considered optical retardance angle from the polarimeter mathematical model.

$$X = \frac{1}{2} \begin{pmatrix} 1 & \cos\delta_1 & \sin\delta_1 \\ 1 & \cos\delta_2 & \sin\delta_2 \\ 1 & \cos\delta_3 & \sin\delta_3 \\ 1 & \cos\delta_4 & \sin\delta_4 \end{pmatrix} = \frac{1}{2} \begin{pmatrix} 1 & 1 & 0 \\ 1 & 0 & 1 \\ 1 & -1 & 0 \\ 1 & 0 & -1 \end{pmatrix}$$

(14)

As a result, we obtained the modulation tensor shown in Figure 10.
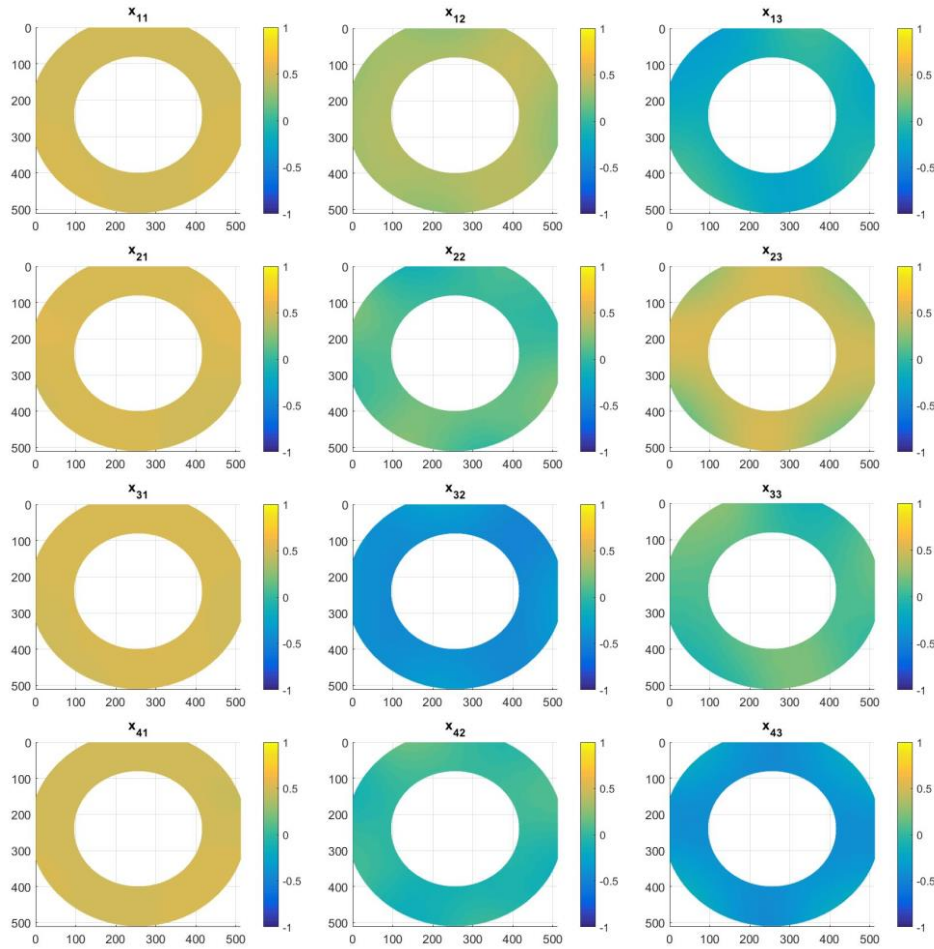
Figure 10 : Computed modulation tensor

Table 2 reports, for each modulation matrix element, the theoretical value, the mean value and the standard deviation obtained considering all the pixels within the images. As it is possible to notice, the obtained mean values are not exactly the same of the theoretical, but result consistent within the uncertainty.

Table 2 : Statistics of the modulation tensor

Modulation Matrix Element	Theoretical value	Mean of computed values	Standard Deviation of computed values
x_{11}	0.5	0,49	0,01
x_{12}	0.5	0,35	0,04
x_{13}	0	-0,14	0,09
x_{21}	0.5	0,51	0,02
x_{22}	0	0,08	0,07
x_{23}	0.5	0,42	0,07
x_{31}	0.5	0,51	0,01
x_{32}	-0.5	-0,42	0,04
x_{33}	0	0,08	0,08
x_{41}	0.5	0,49	0,01
x_{42}	0	-0,02	0,06
x_{43}	-0.5	-0,36	0,06

The theoretical demodulation matrix (15) is obtained by inverting the modulation matrix (14).

$$X^+ = \frac{1}{2}\begin{pmatrix} 1 & 1 & 1 & 1 \\ 2 & 0 & -2 & 0 \\ 0 & 2 & 0 & -2 \end{pmatrix}$$ (15)

As a consequence, by inverting the modulation, it is possible to retrieve the demodulation tensor. Figure 11 reports the obtained results. As it is possible to see, we considered only the demodulation tensor elements comprised in a range between -2 and 2.
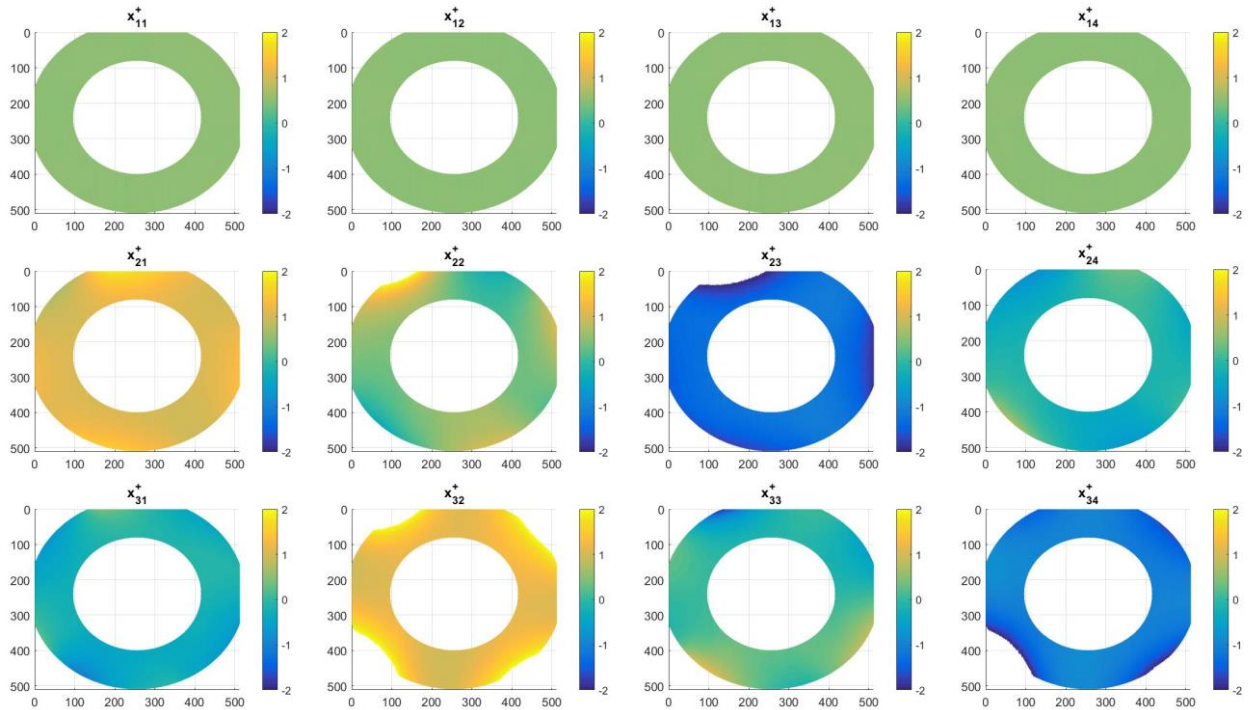
Figure 11 : Computed demodulation tensor

Table 3 reports, for each modulation matrix element the theoretical value, the mean value and the standard deviation obtained considering all the pixels within the images. As it is possible to notice, the obtained mean values are not exactly the same of the theoretical, but result consistent within the uncertainty.

Table 3 : Statistics of the demodulation tensor

Demodulation Matrix Element	Theoretical value	Mean of the computed value	Standard Deviation of the computed values
x^+_{11}	0.5	0,50	0,00
x^+_{12}	0.5	0,50	0,00
x^+_{13}	0.5	0,50	0,00
x^+_{14}	0.5	0,50	0,00
x^+_{21}	1	1,12	0,15
x^+_{22}	0	0,47	0,38
x^+_{23}	-1	-1,39	0,25
x^+_{24}	0	-0,19	0,24
x^+_{31}	0	-0,29	0,20
x^+_{32}	1	1,35	0,34
x^+_{33}	0	0,06	0,33
x^+_{34}	-1	-1,16	0,31

The last step is represented by the computation of the efficiency map associated with the retrieved demodulation matrix, which is the figure of merit to determine the optimum demodulation matrix.

The Metis polarimeter is a particular case where the modulation efficiency of the circular polarization is not relevant and the maximum polarimetric efficiency for linear polarization (Q and U) is required. As a result, the efficiency vector is described by equation (16).

$$\varepsilon_i = \left[\sum_{j=1}^{3} (X_{ij}^{-1})^2 \right]^{-1/2} \tag{16}$$

The maximum efficiency vector for a complete Stokes polarimeter is reported in (17).

$$\varepsilon_{max} = \left(1 \quad \frac{1}{\sqrt{2}} \quad \frac{1}{\sqrt{2}} \right) \approx (1 \quad 0.707 \quad 0.707) \tag{17}$$

Figure 12 shows the values of the efficiency vector elements for each pixel of the analyzed area, while the related statistics is reported in Table 4.
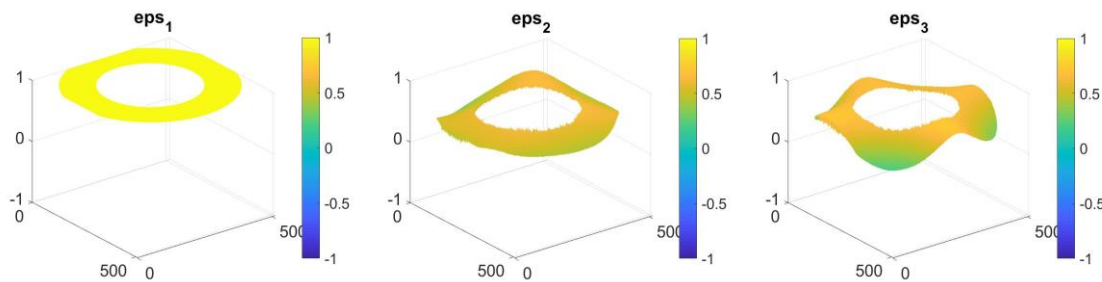
Figure 12 : Efficiency vector map

Table 4 : Statistics related to the efficiency vector elements

Efficiency Vector Element	Theoretical value	Mean of the computed value	Standard Deviation of the computed values
ε_1	1	1.000	2.05e-05
ε_2	0.707	0.537	0.073
ε_3	0.707	0.568	0.110

8.   RESULTS VERIFICATION

In order to verify the validity of the retrieved demodulation tensor, we applied it to data acquired in vacuum, the VL imaging of the "Sun-disk". In particular, the Stokes vector associated with the incoming light can be retrieved by multiplying the obtained demodulation tensor by a vector composed of 4 measured values and acquired applying four different voltages to the PMP cells. As a consequence, for each position of the pre-polarizer we expect to retrieve the theoretical Stokes vector associated with the well-known polarized incoming light. Figure 13 and Figure 14 shows the results obtained by applying the demodulation matrix to the data acquired during the Sun-disk VL imaging test.
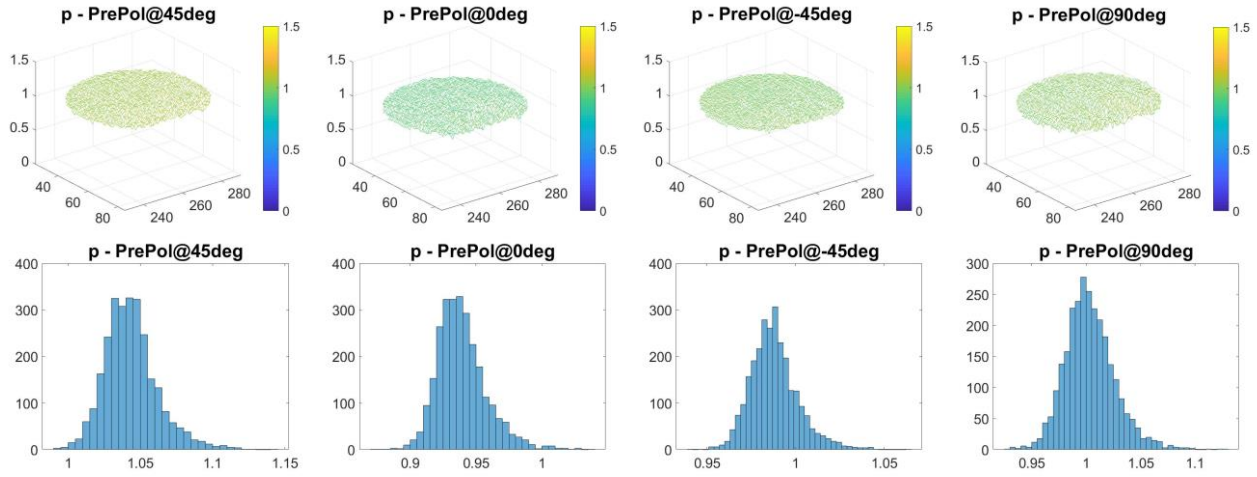
Figure 13 : Retrieved polarization and statistics
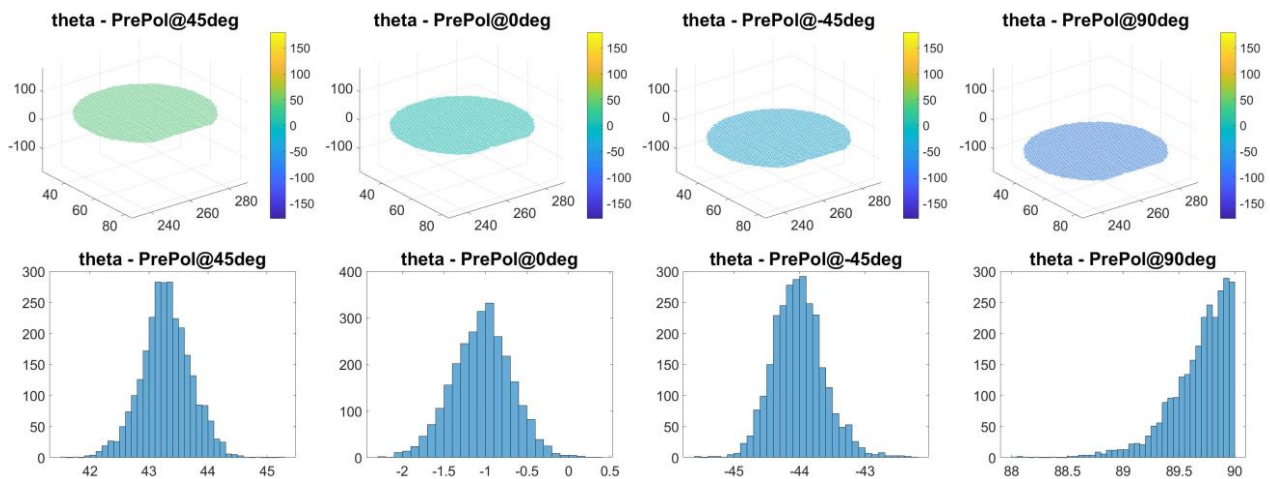
Figure 14 : Retrieved pre-polarizer position and statistics

Table 5 reports, for each image, the statistics.

Table 5 : Statistics related to the demodulation map verification

Pre-Pol Position [deg]	p : Theoretical value	p: Mean	p: Standard deviation	θ : Theoretical value [deg]	θ: Mean [deg]	θ: Standard deviation [deg]
45	1	1,04	0,02	45	43,29	0,42 (~ 0,01 rad)
0	1	0,94	0,02	0	-1,04	0,36 (~ 0,01 rad)
-45	1	0,99	0,01	-45	-44,01	0,39 (~ 0,01 rad)
90	1	1,00	0,02	90	89,68	0,27 (~ 0,01 rad)

9.   CONCLUSIONS

This paper describes the Metis coronagraph calibration campaign related to the polarimetric visible light path. The calibration activities performed on the visible light path of the Metis coronagraph aimed at imaging the "Sun-disk" by characterizing the VL polarimetric response of the instrument and evaluating the instrumental polarization. Two different set-ups have been used. From the analysis of the first acquired set, we retrieved the optical retardance angle – voltage relationship. On the other hand, using the flat-field imaging we retrieved the demodulation tensor associated with the polarimetric VL channel. Lastly, the computed demodulation tensor has been applied to the first dataset, in order to verify the data analysis outcome.

10. ACKNOWLEDGMENTS

REFERENCES

[1]   F. Bernhard et al., "10 years of SOHO", ESA Bulletin, No. 126, p. 24-32, May 2006
[2]   E. Marsch, E. Antonucci, P. Bochsler, J.-L. Bourgeret, R. Harrison, R. Schwenn, J.-C. Vial, B. Fleck, R. Marsden, O. Pace, M. Coradini, "Solar Orbiter", Assessment Study Report, ESA-SCI (2000) 6, 2000
[3]   D. Müller, R.G. Marsden, O.C. StCyr, H.R. Gilbert, "Solar Orbiter Exploring the Sun-heliosphere connection", Solar Physics, 285, 25, 2013
[4]   G. Naletto et al, "METIS, the Multi Element Telescope for Imaging and Spectroscopy for the Solar Orbiter mission", proc. of ICSO Conference, Oct. 2010
[5]   E. Antonucci; S. Fineschi; G. Naletto; M. Romoli; D. Spadaro; G. Nicolini; P. Nicolosi; L. Abbo; V. Andretta; A. Bemporad; F. Auchère; A. Berlicki; R. Bruno; G. Capobianco; A. Ciaravella; G. Crescenzio; V. Da Deppo; R. D'Amicis; M. Focardi; F. Frassetto; P. Heinzel; P. L. Lamy; F. Landini; G. Massone; M. A. Malvezzi; J. Dan Moses; M. Pancrazzi; M.-G. Pelizzo; L. Poletto; U. H. Schühle; S. K. Solanki; D. Telloni; L. Teriaca; M. Uslenghi, "Multi element telescope for imaging and spectroscopy (METIS) coronagraph for the Solar Orbiter Mission" Proc. SPIE 8443, (2012).

[6]   Alvarez-Herrero, A., et al., "The polarization modulators based on liquid crystal variable retarders for the PHI and Metis instruments for the Solar Orbiter mission", proceeding 66598 at International Conference on Space Optics (ICSO 2014)

[7]   M. Romoli et al., METIS: the visible and UV coronagraph for Solar Orbiter, Int'l Conf. Space Opt., 2014

[8]   S. Fineschi, et al., "Novel Optical Designs for Space Coronagraphs: Inverted Occulters and Lyot-stops," Presentation at International Conference on Space Optics ICSO Conference, 2010.

[9]   G. Crescenzio et al, "Imaging polarimetry with the METIS coronagraph of the Solar Orbiter Mission", Proc. SPIE 8443, (2012)

[10]   S. Fineschi, G. Crescenzio, G. Massone, G. Capobianco, L. Zangrilli, E. Antonucci, and F. Anselmi, OPSys: optical payload systems facility for testing space coronagraphs, Proc. SPIE 8148, p. 81480W, 2011. doi:10.1117/12.897794

[11]   M. Casti; S. Fineschi; G. Capobianco; F. Landini; M. Romoli; E. Antonucci; V. Andretta; G. Naletto; G. Nicolini; D. Spadaro; A. Alvarez-Herrero; P. Garcia-Parejo; M. Marmonti, "Calibration of the liquid crystal visible-light polarimeter for the Metis/Solar Orbiter coronagraph", Proc. SPIE 10698, (2018)

[12]   J. C. del Toro Iniesta and M. Collados, "Optimum Modulation and Demodulation Matrices for Solar Polarimetry," Appl. Opt. 39, 1637-1642 (2000)